Facility for studying spin dependence in pion production near threshold

T. Rinckel[1], P. Thörngren Engblom, H.O. Meyer, J.T. Balewski , J. Doskow, R.E. Pollock, B. von Przewoski, F. Sperisen

Department of Physics, Indiana University and Indiana University Cyclotron Facility, Bloomington, Indiana 47408

W.W. Daehnick, R.W. Flammang, Swapan K. Saha[2]

Department of Physics, University of Pittsburgh, Pittsburgh, Pennsylvania 15260

W. Haeberli, B. Lorentz, F. Rathmann[3], B. Schwartz, T. Wise

Department of Physics, University of Wisconsin-Madison, Madison, Wisconsin 53706

P.V. Pancella

Western Michigan University, Kalamazoo, Michigan 49008

Abstract

We describe an experimental setup for the measurement of polarization observables in pion production near threshold. Experiments carried out with this facility use a polarized proton beam in the Indiana University Cooler storage ring, and an internal, polarized hydrogen target. The detector system measures energy, direction and velocity of multiple outgoing charged particles that are within a forward cone of about 32° opening angle. An array of scintillators also allows the detection of neutrons. In addition to the technical details of the apparatus, we describe the procedure for data acquisition, as well as some aspects of the analysis.

[1] Corresponding author: FAX +812 855 6645, e-mail rinckel@iucf.indiana.edu
[2] permanent address: Bose Institute, Calcutta 700009, India
[3] present address: Physikalisches Institut der Universität Erlangen-Nürnberg, 91058 Erlangen, Germany; working at Forschungs Zentrum Jülich GmbH, 52425 Jülich, Germany.

1 Introduction

When electron cooling of a 200 MeV proton beam was demonstrated at Fermilab [1], it became clear that this new technology (for a review see [2]) would benefit medium-energy nuclear physics experiments, because it would make it possible to use an accumulated, stored beam on an internal target in a mode where the target "heating" is compensated by cooling. A storage ring, which exploited this technique, was subsequently constructed at the Indiana University Cyclotron Facility (IUCF) becoming operational in 1989. Since then, a great deal has been learned about the new experimental environment, and other storage rings with phase-space cooling have been constructed in Europe and Asia [3] [4].

The new technology had an important impact on the study of pion production reactions close to threshold. Here the ring environment offers several crucial advantages: the small momentum-spread of the cooled beam is needed because of the rapidly varying near-threshold cross section, the pure window-less internal target drastically reduces background due to unwanted reactions, and the fact that an intense beam can be accumulated and stored compensates for the low target thickness.

Pion production in NN collisions is an interesting process because it is dominated by the short-range part of the NN interaction. The new technology allowed a measurement of the total cross section in $pp \to pp\pi^0$ sufficiently close to threshold [5] [6] to determine the strength of the only remaining amplitude (${}^3\mathrm{P}_0 \to {}^1\mathrm{S}_0$, $l_\pi = 0$). At the time of the experiment, theory was unable to explain the new precise cross section measurements. This unexpected disagreement subsequently inspired considerable theoretical activity, as summarized in ref. [7] [8]. More amplitudes come into play when the bombarding energy is raised. To study these new amplitudes, additional experimental information is required, and the need arises to measure polarization observables.

Over the past five years the PINTEX [4] group has staged an experiment at the Indiana Cooler to measure the spin dependence of the pion production cross section, using a polarized beam and a polarized target. The purpose of the present paper is to describe the technical aspects of this experiment, i.e. to collect information on details of the apparatus and the procedures employed.

The experiments described in this paper were carried out with a stored polarized proton beam interacting with an internal polarized proton target mounted in the A region of the Indiana Cooler (cf. fig. 1). Section 2 describes how polarized beam is stored in the Cooler and what determines its polarization. Section 3 describes the polarized target, properties of the target cell and how

[4] Polarized INternal Target EXperiments: www.iucf.indiana.edu/~pintex

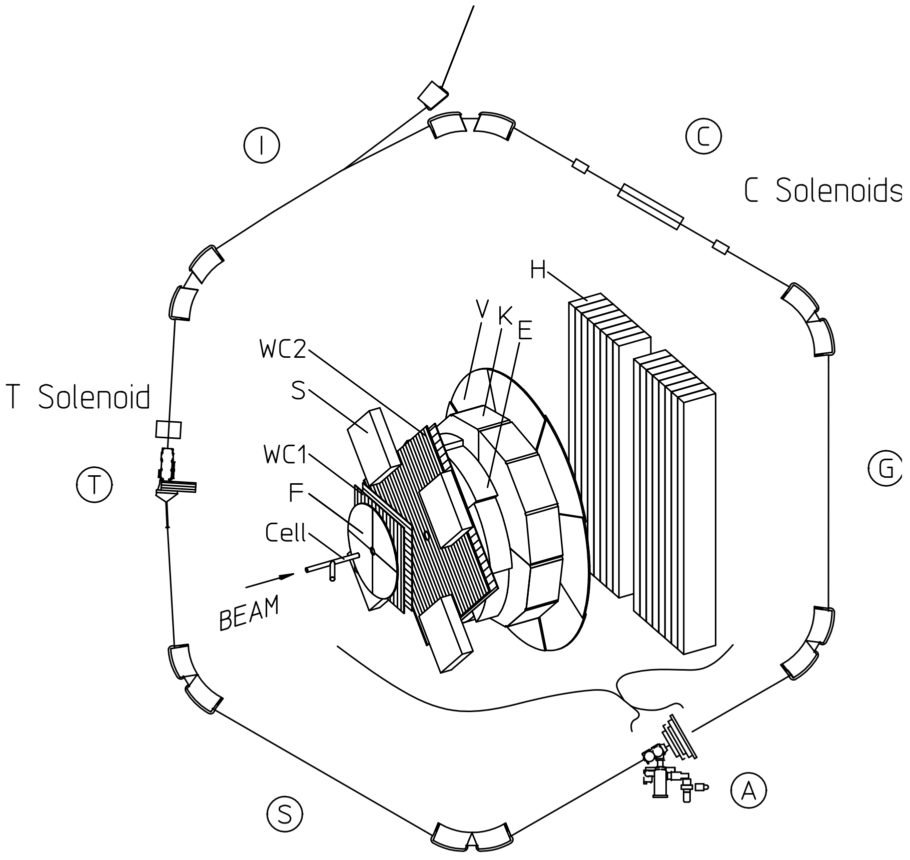

Fig. 1. Overview of the Cooler, a storage ring and synchrotron for polarized protons and deuterons, with a circumference of 86.77 m. The straight sections referred to in the text: A) The PINTEX experimental area. C) Electron cooling section. T) T solenoid. I) Injection point. The maximum proton energy is 500 MeV. Detailed insert shows the Forward Detector Stack (items F through K) and the Hodoscope (H). The individual elements are described in more detail in section 4.

the target polarization is changed.

The reaction $pp \to pp\pi^0$ is identified by measuring the four-momentum of the two outgoing protons. The detector system (see fig. 1), described in section 4, consists of 5 scintillator planes and 4 wire chamber planes that cover all of the phase space of the final state with the exception of the small-angle region occupied by the beam pipe. The scintillators are segmented so that two elements firing signify a possible candidate for the reaction $pp \to pp\pi^0$. The reactions $pp \to d\pi^+$ and $pp \to pn\pi^+$ were measured in a similar fashion via the coincidence of the charged particles, or the coincidence between a stopped proton and a neutron in the hodoscope (H in fig. 1). Beam polarization, target polarization and the luminosity was monitored via pp elastic scattering near 45° in the lab, measured concurrently with pion production. Section 5 discusses the readout system for these detectors, the different event types that are processed and the typical data-taking cycle.

Section 6 discusses the event reconstruction. Tracks are reconstructed from wire chamber hit patterns. Corrections are made to the raw signal sources for light collection. The light output is converted into energy and the missing mass of the undetected particle is calculated. These missing masses are then sorted by beam and target spin state combinations. Section 6 also discusses calculating the beam and target polarizations and luminosity from the 45°detectors. Section 7 discusses corrections to the data due to detector acceptance and backgrounds. Section 8 summarizes the system and gives an outlook on its advantages.

2 Polarized Beam

2.1 Generation, Accumulation and Storage

Polarized protons from a polarized ion source [9] are accelerated in the Injector and the Main Cyclotron to 197 MeV, and delivered to the injection point of the Cooler (I in Fig. 1). Kick-stack injection, assisted by electron cooling [10] is then used to accumulate stored beam in the Cooler. After filling for 2-3 minutes, the stored beam energy is ramped to the desired final value. Average orbiting beam currents are 100-200 μA. After data taking for 5-8 minutes the beam is discarded. For the next fill, the reversed spin state is injected into the ring. The beam polarization is between 0.65 and 0.70.

The magnetic moments of stored particles precess around the magnetic fields in the ring. Depolarizing resonances occur when this precession is consonant with the particle motion around the ring. In the Cooler, a so-called intrinsic depolarization resonance exists just below the injection energy of 197 MeV, when the relation $G\gamma = 7-\nu_y$ is satisfied (G is the proton anomalous magnetic moment, γ is the relativistic Lorentz factor, and ν_y is the vertical betatron tune). Since a tune change of only 0.02 increases the polarization lifetime from minutes to days [11] this resonance is easy to avoid. There are no other important depolarizing resonances between 200 and 500 MeV. Under these conditions, accelerating the beam has no significant effect on its polarization [12]. This fact has been used to establish a calibration standard across the energy range of the Cooler. The calibration information has the form of analyzing power and spin correlation coefficients in pp elastic scattering from 200 MeV to 450 MeV [13]. Since pp scattering is used to monitor beam and target polarization concurrently with pion production (see sects. 4, 6), the absolute scale of polarization observables in the latter reaction was set.

2.2 Non-Vertical Beam Polarization

Typically, the stable spin direction in a storage ring is vertical. To get longitudinal beam polarization at the target in the A region, spin-precessing solenoids are added to the Cooler lattice. We chose an economical scheme which makes use of three solenoids that are already present in the electron-cooling system in the C region (see fig. 1), and a newly installed superconducting solenoid in the T region.

The three solenoids in the C region are normally operated in compensating mode (vanishing longitudinal field integral). When these solenoids are operated with their fields all parallel, a maximum field integral of 0.88 Tm can be achieved. The superconducting solenoid installed in the T region has a maximum field integral of 2.0 Tm at 90 A. The short effective length (35 cm) of the magnet causes relatively strong focusing of the beam which must be compensated by adjustments in the ring quadrupole magnets.

For guidance on ring quadrupole adjustments necessary to run the Cooler with the C and T solenoids, their effects on the beam were studied using the CERN MAD [14] program. While the effects of the C solenoid were found to be relatively small (consistent with our experience during an initial test run), running the T solenoid above 1 Tm would require significant changes of a large number of quadrupole strengths. The predicted quadrupole changes were borne out qualitatively during commissioning. The transverse ring acceptance appeared to be little affected, while a slight decrease in the accumulation rate was observed. Since it proved to be difficult to run the Cooler with T solenoid strengths in excess of 1.1 Tm, the C and T solenoid fields were kept fixed at 0.88 and 1.10 Tm, respectively.

At the injection energy of 197 MeV, the beam polarization at the target is mainly longitudinal (96% of the injected polarization from the cyclotron). This happens to correspond to a nearly vertical stable spin direction at the injection point (I-region), thus no spin precession was required prior to injection. Longitudinal beam polarization was used for a measurement of A_{zz} in $\vec{p}\vec{p}$ elastic scattering 197 MeV [15]. Since the solenoid fields are fixed when accelerating the beam, only partial longitudinal polarization is available for the pion production experiments. For instance, at 400 MeV, the beam polarization components at the target are 0.59P longitudinal, 0.10P sideways, and 0.80P vertical where P is the magnitude of the beam polarization.

3 Polarized Internal Target

3.1 Atomic Beam Source

Polarized hydrogen atoms from an atomic beam source are injected into a target cell (see below). To produce the polarized atoms, first a slow atomic beam is generated using a dissociator with a cold nozzle. This beam then passes through the inhomogeneous field of a sextupole magnet which defocuses two of the four possible hyperfine states. Subsequently, RF fields are used to induce a transition between spin states, followed by another sextupole magnet, which focuses a pure atomic spin state. The atomic beam source employed in this experiment is described in ref. [16]. Details about the RF transition unit can be found in ref. [17]. The atomic beam at the entrance of the fill tube of the cell has a diameter of about 10 mm and an intensity of 6×10^{16} atom/s [16].

3.2 Target Cell

When the atomic beam is injected into a storage cell [18], the target thickness increases by a factor of several hundred [19] compared to just using the atomic beam itself. The target cell consists of an open-ended tube through which the stored beam passes, with a fill tube attached to the side through which the incident atomic beam is directed (see fig. 2) The polarized atoms accumulate in the cell because of the flow impedance along the tubes. The density of the target along the storage cell is triangular reaching zero at the ends of the cell. The thickness of the entire target is a few times 10^{13} atoms/cm^2.

The constraints on the design of such a storage cell are summarized in ref. [20]. Clearly, the narrower the tube, the larger the target thickness. On the other hand, a narrow cell limits the ring acceptance which lowers the beam lifetime and thus also the time-averaged beam current. In addition, a narrow cell may adversely affect the injection efficiency and the ring performance during acceleration and cause background from interactions with the cell wall. These conflicting requirements were studied experimentally prior to the installation of the polarized target [21].

The experiment imposes yet another set of constraints on the cell design, depending on the requirements for the detection of reaction products. For pion production it was desirable to have a low-mass cell so that low energy reaction particles emerging from any point along the cell axis into the detector acceptance are unaffected. Also, it was desirable to have uniformity over the full 360 degrees which rules out any massive supporting elements. In addition, it was mandatory to minimize any material near the beam axis in order to

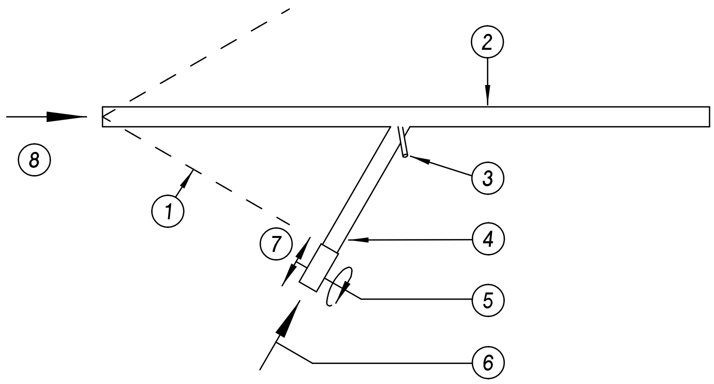

Fig. 2. Storage cell for pion production. 1) 30° unobstructed exit cone. 2) 12 mm diameter 250 mm long beam tube with 25 μm aluminum wall. 3) Fitting to introduce unpolarized gas. 4) 11mm diameter aluminum feed tube with 75 μm wall. 5) Pivot axis for vertical adjustment of cell position. 6) Atomic beam. 7) Translation direction for horizontal adjustment of cell. 8) Stored proton beam.

reduce reactions induced by the halo of the beam that might contribute to experimental background.

The present target cell (fig. 2) is a 12 mm diameter, 250 mm long, tube constructed from 25 μm aluminum foil (grade-1145, 99.45% pure). The foil is wrapped onto a 12 mm diameter copper electrode and spot-welded lengthwise with 0.5 mm overlap. A second 11 mm diameter tube of 75 μm wall thickness machined from solid, grade-1100 aluminum intersects at 30° to the normal and is spot welded to the 12 mm beam tube. By making use of a blocker in the atomic beam, the target atoms can be stopped from entering the storage cell. For tests with a thick, unpolarized target, H_2 gas is fed into the cell through a 1 mm Teflon tube, connected to a small fitting spot-welded to the 11 mm tube close to the fill tube. This cell is self supporting and held in position only by the entrance to the fill tube. Depolarization during the roughly 300 wall collisions is minimized by coating the cell with Teflon dispersion [5] mixed 1:1 with water and then baking it at 380°C for 1 hour [22].

To minimize background from beam halo and to optimize Cooler beam injection and peak beam current it is desirable to allow for transverse remote adjustment of the target position. To this aim, we constructed a motorized cell adjustment mechanism that maintains alignment of the fill tube to the atomic beam. Motion in the vertical (y) direction is achieved by pivoting the cell about the fill tube entrance, as indicated in figure 2. Horizontal (x) motion is achieved by translating the target along the fill tube axis. The component of this motion in the beam direction (z) can be ignored. During beam studies the target may be pivoted entirely out of the ring acceptance. View-ports in-

[5] Teflon type 307A, formerly type 3170, Du Pont Inc.

stalled in the corners bracketing the A-region allow sighting along the beam axis. Making use of this, the position of the target cell is monitored by an astronomical telescope coupled to a video camera located about 8 m upstream of the target.

3.3 Target Polarization

The orientation of the polarized atoms from the source follows adiabatically the direction of the ambient magnetic field, ending up in the direction of the guide field established at the target cell. This guide field, generated by one of three orthogonal Helmholtz-type coils, has to be strong enough to overcome the ambient field in the room but small to not affect the stored beam. To minimize interference with the stored beam, compensating fields are established just upstream of the target as well as 0.6 m downstream (see ref. [23] for more details). The guide field coils are arranged to provide a field in the x, y and z direction. The corresponding field strengths used are $B_x = \pm 0.25$ mT, $B_y = \pm 0.33$ mT and $B_z = \pm 0.60$ mT. These values are offset by a small amount to cancel the ambient field. Reversing the current in the coils changes the sign of the target polarization. A sign change takes less than 10 ms [24]. During a measurement, data are acquired in sequence for all target polarization directions (see sect. 5). A bit pattern that describes the current polarization direction is recorded with each event.

Except for the need to de-ice the dissociator nozzle by warming it up every 3-4 days, the polarized target facility performed without interruption over the duration of a run (typically 10 days). During this time, the target polarization was stable and typically 0.70 - 0.75.

4 Detector setup

4.1 Main Scintillator Detectors

The purpose of the main scintillators in the detector stack (marked F, E, K and V in figures. 1, 3, 4) is to generate a fast trigger for pion production, to measure the kinetic energy of stopped, charged particles, and to determine the time of flight of these particles in order to distinguish between charged pions, protons, and deuterons. The detector stack is located immediately downstream of the "exit window" (EW), which represents the downstream end of the vacuum chamber. The exit window, indicated in figure 3, consists of a 0.18 mm thick stainless steel foil which is brazed to the beam pipe, having inner and outer

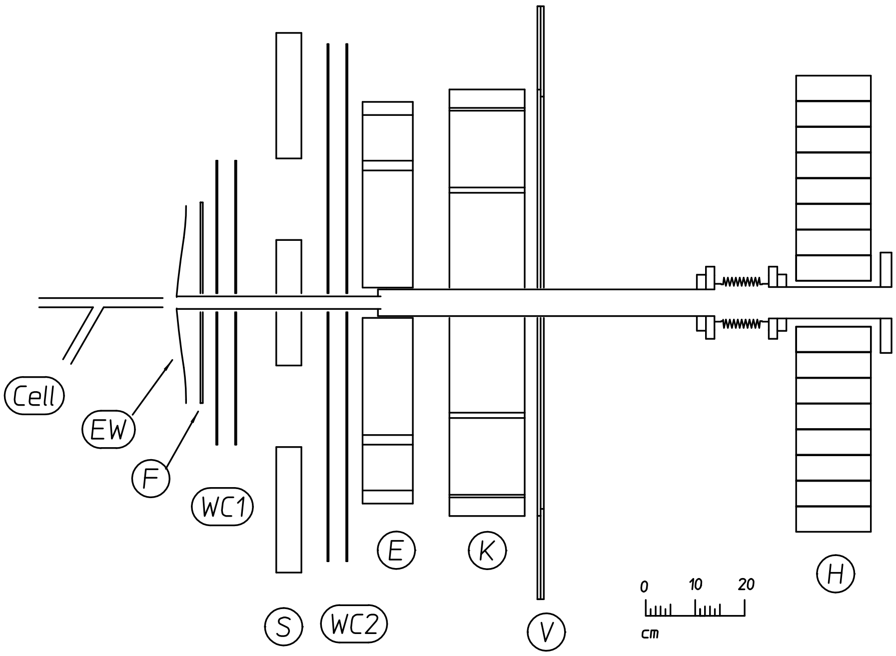

Fig. 3. Top view of detectors.

radii of 13 mm and 206 mm. The main scintillators are cylindrically symmetric, segmented arrays, as shown individually in figure 4. In the following, r_i and r_o denote the inner and outer boundary of the sensitive area of the detector arrays.

The purpose of the "Front Detector" (F) is to provide a start signal for the time-of-flight measurement. The detector is placed as close to the exit window as possible in order to exclude particles in the beam halo that scatter from the beam pipe downstream of the window. The F detector is made from 1.5 mm thick BC408 (Bicron[6]) scintillator, and its dimensions are $r_i = 16$ mm and $r_o = 203$ mm. The segments of the F detector are slightly overlapping. From particle tracks that fire two adjacent F segments, the average time resolution was determined as 1.4 ns.

The "E-detector" (E) is the first of two thick scintillator arrays, designed to stop charged particles after pion production. The detector has eight-fold segmentation, allowing particles to be detected in coincidence and is made from 103 ± 2 mm thick BC408 scintillator material of dimensions $r_i = 38$ mm and $r_o = 369$ mm. Each of the eight segments is coupled to two Amperex XP2041 photo-multipliers. The position dependence of the light-collection efficiency was measured and is corrected for during the analysis (see sect. 6).

A second layer of stopping scintillator is provided by the "K-detector" which

[6] www.bicron.com

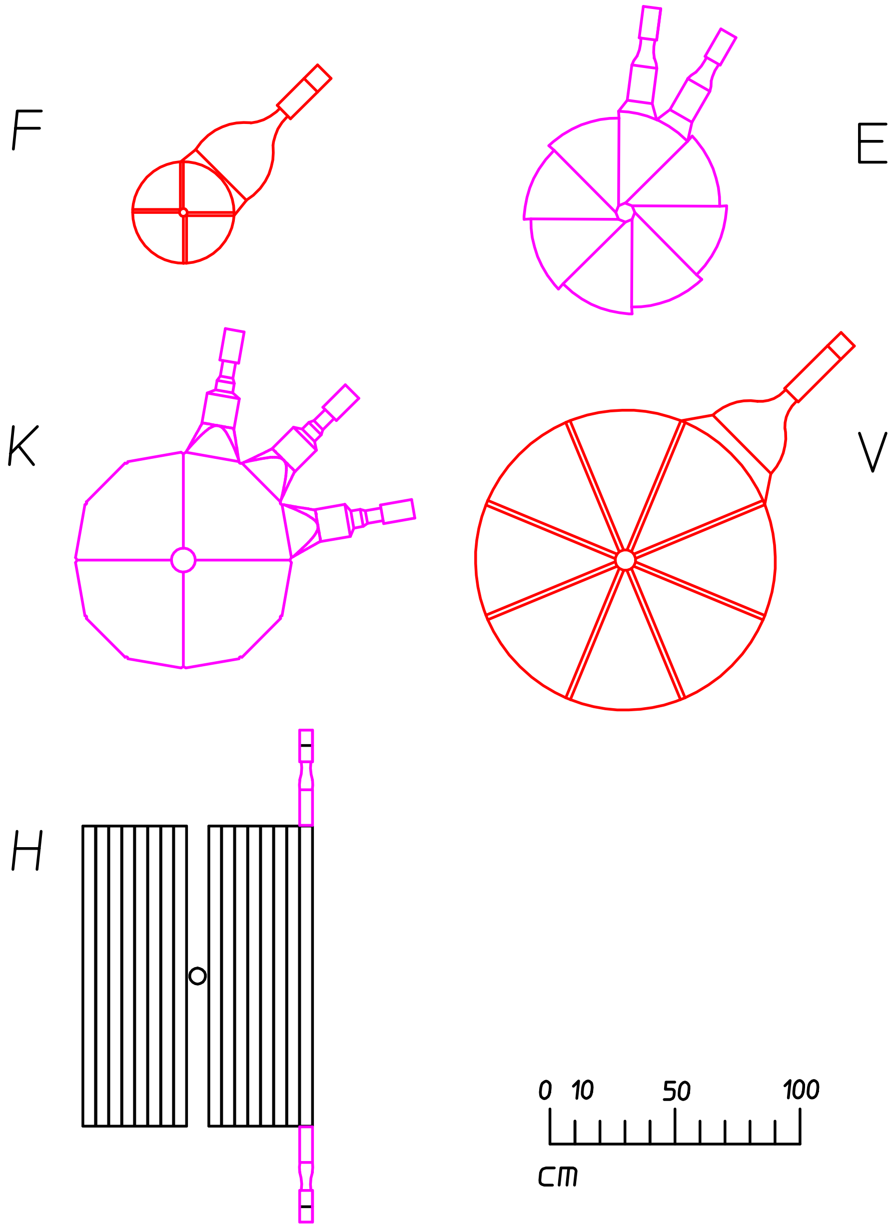

Fig. 4. The figure shows the segmented pattern of the scintillator detectors. The dashed lines indicate an overlap between adjacent sectors. The light collection arrangement is only illustrated on one segment for each detector.

was constructed by the group at the Western Michigan University (Kalamazoo). The K detector, together with the E detector, stops protons from pion production at bombarding energies up to 400 MeV. The K detector is made from 152 ± 2 mm thick BC400 scintillator material, and its dimensions are r_i = 48 mm, r_o = 423 mm. Each of the four segments is coupled to three Hamamatsu R1250 photo-multipliers. The sum of the outputs of the three gain-matched photo-tubes gives a signal proportional to the energy deposited in the scintillator. Simulations show that light collection efficiency varies not more than 5% from one part of the segment to another. The remaining position dependence of the light-collection efficiency was measured and corrected for during the analysis (see sect. 6).

The veto detector (V) is used to confirm that a given charged particle has stopped in the preceding E and K detectors. It is also used in conjunction with the neutron detector (see 4.4). Most of the particles striking the veto detector are beam-energy protons elastically scattered in the target gas or target cell. The V detector is made from 6.4 mm thick BC408 scintillator material, and its dimensions are $r_i = 41$ mm and $r_o = 610$ mm. The segments overlap to eliminate any cracks in the veto coverage.

4.2 Wire Chambers

The purpose of the wire chambers is to establish the directions of multiple charged-particle tracks. There are two units, each containing two wire planes with wires running orthogonal to each other (see figs. 1 and 3). In the first unit (WC1) the wires are vertical and horizontal. The second unit (WC2), further downstream and thus larger, has wires running at 45° to the vertical to resolve ambiguities with multiple tracks. The wire chambers are of an unique design featuring a hole in the center in order to admit the beam pipe [25].

The WC1 chamber has two planes with 144 wires each and 3.18 mm wire spacing. The planes are separated by 9.5 mm. The smallest and largest circles within the sensitive region have radii of 18 and 235 mm, respectively. The WC2 chamber has two planes with 112 wires each, with 6.35 mm wire spacing. The planes are separated by 22.2 mm. The inner and outer radius of the sensitive region are 50 and 370 mm. The operating voltage is -2.4 and -2.9 kV for WC1 and WC2, respectively. While the beam is injected or discarded the voltage is lowered by a factor of two in order to avoid surges in the anode current.

The efficiency for a single plane (i.e. the probability that a charged particle is registered) is estimated from data gated with the E and F scintillators in coincidence and one cluster in the other chamber. It varies between 93 and 95% for each of the four planes. Thus, a single prong event results in one cluster in *each* of the four planes with 75-82% probability. The overall wire chamber efficiency for two prong events has been calculated taking into account that events with one cluster missing or one or two multiple hits can still be recovered. The expected total efficiency is then 90-94%.

4.3 45° *Detectors*

Elastic pp scattering events near $90^\circ_{\mathrm{c.m.}}$ are observed concurrently with pion production in order to determine the product of beam and target polarization (P·Q) and the luminosity (see sect. 6.3). Scattered protons in the angular range $37^\circ \leq \theta_{\mathrm{lab}} \leq 47^\circ$ are detected as coincidences between two opposite elements of scintillators (labeled S in figs. 1, 3). The scintillators measure 254 mm × 254 mm × 51mm thick, and are made from BC408 scintillator material. They are placed immediately in front of the second wire chamber (WC2) at azimuthal angles ±45° and ±135° with the inner edge 292 mm from the beam axis (see fig. 3). Since elastically scattered particles go through the outer corners of WC1, tracking information is available (see sect. 6).

4.4 Neutron Hodoscope

The purpose of the neutron detector is to measure the process $pp \to pn\pi^+$ by detecting a neutron in coincidence with a stopped proton. The neutron hodoscope (H in fig. 3) consists of 16 bars of BC408 scintillator material. Each bar is 51 mm wide, 151 mm deep and 120 cm long. The bars are placed closely packed, in a vertical orientation, in two groups of eight, on both sides of the beam. The distance from the inner edge of either group to the beam axis is 75 mm. The upstream face of the hodoscope is 147 cm from the center of the target cell. Each end of each bar is coupled, through a 15 cm long light guide, to a fast Amperex XP2252/h photo-multiplier. The x and y position of a neutron hit is deduced from the bar number (resolution given by the bar width) and from the time difference between signals at opposite ends of a given bar (resolution 4 cm FWHM). The neutron velocity is deduced from the difference between the time of the F detector pulse and the mean of the time of the pulses at opposite ends of a bar (with a correction for the proton travel time to the F detector). The achieved neutron time of flight spread is $\sigma = 0.09$. Details of the construction and performance of the neutron hodoscope have been given in a previous publication [26].

Neutron energies of interest range from 21 to 228 MeV. The efficiency of the neutron detector depends on the threshold setting. The gains and thresholds are adjusted to obtain the same efficiency for all bars. For this purpose, cosmic ray muons that traverse at least 6 bars are recorded concurrently with data taking. Using a 5 MeV threshold the detection probability is 17% for 30 to 50 MeV neutrons and 13% for 50 to 200 MeV neutrons. Interactions with the material between the target and neutron detector lowers these figures to 5% and 9%, respectively.

5 Data acquisition

5.1 Signal Processing

The PINTEX detector system includes six scintillator arrays with a total of 76 photo-tubes. LeCroy [7] remote-controlled high voltage mainframes supply the operating voltage to the photo-tubes. Throughout, bases with transistor-stabilized bias of the last three stages are used. The anode signal of each photo-multiplier is amplified in order to keep the operating voltage of the photo-multipliers low which lowers the recovery time of the photo-tube. The amplifier outputs are sent to a discriminator LeCroy 4413 and a LeCroy FERA ADC. The ECL outputs of the discriminator are fed via LeCroy 4418 programmable delay modules, into the logic matrix and into TDC's (LeCroy Time-to-FERA converter followed by a FERA ADC).

The event triggers are defined by a group of remotely programmable, ECL-logic CAMAC modules, including seven LeCroy 2365 Octal Logic Modules (OLMs) and a pattern analyzing LeCroy 2732 Memory Lookup Unit (MLU). The logic operations are performed in steps. In the first step, an OR is formed of all scintillators in a given array. In the next step, if the logic conditions for a given event stream are satisfied a "possible event" signal is generated. This signal, which occurs about 120 nanoseconds after an event occurs, sets the busy flag, generates gates for the ADC's and the coincidence registers and starts the TDC's. In the last step, the MLU is queried to decide if this event has the correct scintillator pattern and is really wanted. If yes, a trigger is issued, if no, the busy flag and all CAMAC units are cleared for the next event. The function of the programmable electronics modules is defined by a setup file which is interpreted and down-loaded within seconds. Thus, changes of thresholds, delays and trigger conditions are quick, easy and possible by remote control.

The four wire chamber planes feature a total of 512 wires. A binary signal from each wire is processed by LeCroy 4448 ECL coincidence registers. Some wires near the center are split by the hole for the beam pipe. The signal from the two halves are OR-ed, to simplify readout and processing. The hit pattern from the registers is simplified by the VME processor (see below). The information which is transmitted consists of the centroid and width of "clusters" where a cluster is a consecutive group of wires that have fired.

The neutron hodoscope electronics uses NIM modules. Fast pulses from the 32 photo-multipliers (top or bottom) are fed into constant fraction discriminators

[7] www.LeCroy.com

(ORTEC[8] CF8000). Their output is sent to ADC's and TDC's and a logic signal is generated which announces an event in the neutron detector. This signal enters the logic matrix at the last step.

The CAMAC modules are controlled by a Motorola[9] 68040 CPU in a VME crate through a CAMAC branch driver. The FERAs are read out through their FERA bus directly into a VME dual-port memory module. The coincidence registers are read out through standard CAMAC. The VME processor is programmed to read and reset the CAMAC modules, to scan the wire chamber hit pattern for clusters and widths, to prepare an event for transfer, to buffer the data, and to send the buffers via Ethernet to the HP host computer. The host computer then writes the raw events to tape, and sorts the data into histograms. A typical event contains 70 words. Under this condition, the live time of the VME system is 70% at a processed data rate of 1kHz.

5.2 Event Types

The trigger logic produces signals for four different types of events. Upon receipt of a trigger, the CAMAC modules are read. For simplicity and for diagnostic purposes, ALL modules are read, independent of event type. Triggers have been defined for the following conditions (listed in the order of decreasing priority, see figure 3 for detector labels).

"Pion Trigger". The condition for a "possible" trigger is a coincidence of one or more F segments with one or more E segments, but no signal in the V detector. This is upgraded to "actual" trigger for one of two reasons: either two or more E segments have fired (as determined by the MLU), or there is a coincident neutron signal. This corresponds to two charged particles stopped in the scintillator stack, or one stopped particle together with a neutron in the H detector.

"Monitor Trigger". The condition for this event is a pulse in either of the upper two 45 degree detectors in coincidence with a pulse in any of the lower two detectors. This includes pp elastic scattering events near 90 degrees which fire opposite detectors. It also includes a coincidence between the left two (or the right two) detectors, which was used for background studies.

"Single-Prong Trigger". The condition for this event is a triple coincidence between one or more segments in the three arrays, F, E, and V. This corresponds to an energetic charged particle, such as a forward scattered proton. These events were acquired for diagnostic reasons. The rate of such coincidences is

[8] www.egginc.com/Inst-138/FrontPage.htm
[9] www.mcg.mot.com

very high. Thus, these events were sampled by also requiring a coincidence with a free-running logic pulser with about 5% duty factor.

"H Cosmic-ray Trigger". The condition for this is a coincidence between the outermost bars in either half of the neutron hodoscope (H). This corresponds to a muon traversing all of the bars. The signal is used to adjust the H detector gains and thresholds for uniform efficiency.

In addition to the triggers listed above, there are a number of utility event types. These are used to start the timing sequence in a cycle (see next sect.), to read the scalars once every second, and to initiate the reset tasks at the end of a cycle.

5.3 Run-time Scenario

The time sequence of the injection, acceleration, cooling and discarding of the beam is set by the Cooler control computer. The time for filling, making use of kick-stack injection while cooling, is of the order of 2-4 minutes. After acceleration the beam becomes available for the experimenters at the beginning of the so called flattop, when the field strength of the dipole magnets are constant. At this point there is a logic pulse issued from the Cooler control computer to start the data acquisition system. A typical duration of the flattop is 8 minutes, decided by the lifetime of the beam which normally is of the order of 30-60 minutes. At the end of every flattop the beam is discarded and at the next injection the beam polarization is reversed.

The structure of the timing of the data-taking is organized in two levels. These so called cycles and sub-cycles are governed by Jorway[10] 221 Timing and Sequence Modules and Jorway 222 TTL Buffer Modules, one as a master and the second as a slave. Five seconds after the start pulse from the Cooler control computer to the data acquisition system the target is turned on by pulling out the blocker which lets the atomic beam into the storage cell, at the same time the high voltage of the wire chambers is raised to the operating value.

The DATA ON flag is set at 13 seconds and one second later the slave Jorway is started that operates the target guide fields. All target spin directions are cycled through ±x, ±y and ±z in sequence. The reason for reversing the guide fields is to present the same experimental conditions to each spin combination of beam and target, thus reducing systematic errors. For each of the beam and target spin states a bit is set. In all, 12 spin bits are needed to determine the combination of beam and target polarization. Each guide field direction is held

[10] Jorway Corp., 27 Bond St., Westbury, NewYork 11590

for a period of 2 s and a full sub-cycle lasts 12.5 s. At every polarization change a target SPIN VALID flag is set off for a duration of 100 ms, the requirement in the analysis that this flag is on ensures that only fully polarized target data is used. This is crucial since it is assumed in the analysis that the target polarization is the same in all directions. This assumption has been verified experimentally[21] [23]. The time constant for a polarization reversal is 7 ± 1 ms [24]. At the end of the flattop, data acquisition is stopped, the atomic beam into the target cell is blocked and the wire chamber high voltages are reduced to standby values.

A flattop of 500 s allows for 38 sub-cycles which means the effective data taking time is 433.2 s for each 500 s cycle.

6 Analysis

6.1 Event Reconstruction

6.1.1 Track Reconstruction

Ideally, an event with two charged particles in the exit channel leads to two hits ("clusters", see sect. 5.1) in each of the four wire chamber planes. In this case, the tracks of the two detected particles are obtained as follows. The parameters of two straight lines are varied in a fit to best represent the measured wire positions. The two lines are constrained as to intercept. The fit criterion to be minimized is the sum of the squares of the distances between the eight wire positions and the two tracks divided by the square of the respective position resolution in the two chambers. The value of this number after minimization, χ^2_{WC} measures how well a given event conforms to a physical two-prong event that originates in the target. The output of the fit consists of the two track directions and the coordinates of the point of origin (vertex).

In reality, there may be fewer than two hits in a given plane (because of wire chamber inefficiency), or there may be more than two hits (because of noise or the presence of an extra particle). Most events with only one hit in one of the planes are recovered since there is still enough information for the fit. In the case of too many hits, all possible combinations are tried and the one with the smallest χ^2_{WC} is retained.

Ideally the wire chamber coordinate system should coincide with the beam axis. Since the closed orbit in the Cooler, and thus the beam position at the target may vary when the beam energy is changed, the position of wire chambers has to be corrected accordingly. The corresponding offset is deduced from the monitor events (pp elastic scattering near $\theta_{\rm lab} = 48°$). Since these events are coplanar, a straight line between the intercepts of the two prongs in the first wire chamber (WC1) crosses the beam axis. Collecting the crossing points between these straight lines for subsequent events thus indicates the beam position, and yields the required horizontal and vertical offsets of the coordinates for both wire chambers (WC1 and WC2). Individual offsets on the order of 0.5 to 5 mm were determined for different energies.

6.1.2 Energy Calibration

The energy of stopped particles is determined from the pulse height in the E and K detectors. Even though these detectors were designed for uniform light collection efficiency, there is a remaining dependence on position of the fraction of the light that reaches the photo-multipliers. To correct for this, the E and K pulse heights are multiplied by a correction factor that depends on the place of intercept of the particle track (determined from the wire chambers) with the front face of the respective detector. The correction factors are stored in a lookup array. Their value is determined from the data using the intrinsic position dependence of charged particle energies as predicted from kinematics and energy loss calculations.

The position-corrected pulse height response is then multiplied by an overall scale factor for each segment in the E or K array, in order to make the response of all segments the same. These scale factors depend on the orientation of the target polarization because the photo-multiplier gain is affected by the fringe of the magnetic target guide field. The gain corrections due to the guide fields were up to $\pm 10\%$, and were largest for the longitudinal (Z) guide field. At this stage, the E and K detector response depends no longer on the track position, nor on the spin state of the target.

Once the light response from the thick scintillators E and K have been adjusted the absolute energy calibration can be done. The energy calibration is done according to

$$E = k_0 + k_1 * (E_{light} + k_2 * (K_{light} + k_3)) \tag{1}$$

where k_0-k_3 are calibration constants, E the calibrated energy and $E_{light}(K_{light})$ corresponds to the light collected in E and K respectively, corrected for position and spin dependence. If K_{light} is zero the offset k_3 is set to zero. Equation 1 could be refined by taking into account non-linear effects due to the quenching interactions that appear among excited molecules at high densities.

The calibration constants k_1-k_3 are determined by calculating the correct mass on the pion, maintaining continuity in the total energy spectrum and mini-

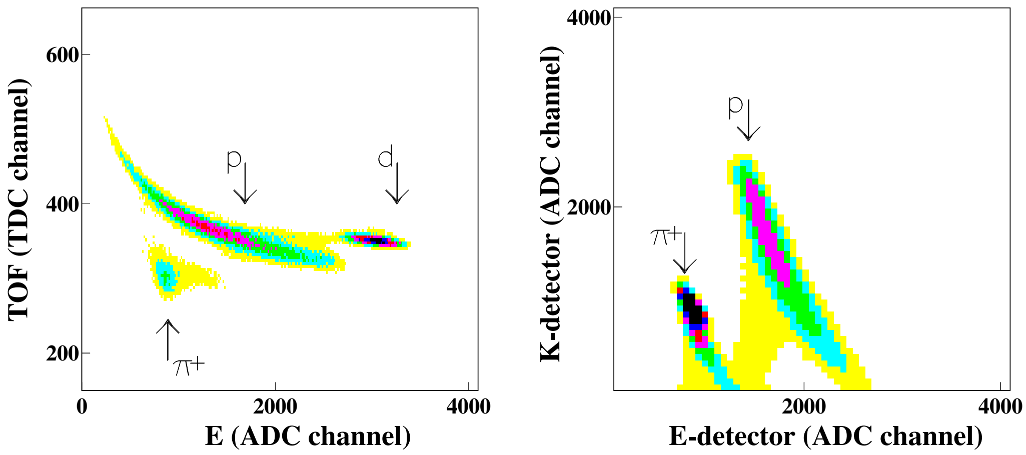

Fig. 5. (left) Time of flight between the E and F detectors versus the energy deposited in the first stopping scintillator. The structures indicated are the deuteron peak from $pp \to d\pi^+$, the banana shape from protons stopped in the E-detector and beneath them pions show up that pass through. (right) E vs. K. Protons from $pp \to pp\pi^0$ that pass through the E-detector are stopped in the K-detector.

mizing the width of the reconstructed missing mass peak. The unpolarized distribution of the θ_{cm} of the pion in the reaction $pp \to pp\pi^0$ is symmetric around 90° in the center of mass because the incoming particles are identical. This distribution is very sensitive to the magnitude of the constant k_0 in the calibration. Adjusting the θ_{π^0} spectrum to be symmetric for the forward and backward going π^0 gives the absolute value of k_0.

The final kinetic energy is then calculated according to

$$E_{kin} = E + E_{loss} \tag{2}$$

where E_{loss} is the calculated energy loss deposited in the material of the detector stack prior to the face of the E-detector.

6.1.3 Particle Identification

The timing signals from the F and the E array are used to determine the particle time of flight. An offset is added to the TDC output of each segment in these arrays, in order to make the timing information independent of which segments fired. These offsets are determined from single-prong events. The start signal from the F detector is synchronized making use of simultaneous fires of adjacent segments which are present because of the small overlap between segments.

For particles that stop in the E-detector, the particle type is identified by time of flight between the E-detector and the F-detector versus the energy deposited in E-detector. For particles that reach the K-detector, clean separation between protons and pions is achieved by setting a gate in the E-energy versus K-energy scatter plot (See fig. 5). The particles from the reaction $pp \to d\pi^+$ can also be identified due to the two-body relationship between the scattering angles.

6.2 Selection of Pion Production Events

The event stream using the "Pion Trigger" (cf. sect. 5.2) corresponds to two charged particles stopped in the forward detector stack, or one charged particle that is stopped and a neutron detected in the hodoscope. The three final states of interest are $pp\pi^0$, $d\pi^+$ and $pn\pi^+$.

The known tracks of the two charged particles are compared to the firing patterns in the F, E and K detector arrays, in order to associate a given element in each of these arrays with either the first or the second prong. In this procedure, the outlines of the detector segments are taken to be about 5mm larger than in reality to account for uncertainties in the track reconstruction. Events for which the match to individual segments is ambiguous are discarded.

The conditions defining a valid two-prong event consist of: 1) Scintillator condition (any F fired, two or more E-segments fired, successful matching between track and scintillators); 2) Accepted wire chamber signatures are 2222, 2221, 2223, 2233, each number denoting the number of clusters in one of the four planes; 3) A condition on the Z coordinate of the reconstructed vertex and a cut in the χ^2 of the kinematic fit; 4) A condition on the opening angle between the two tracks versus the difference between the two azimuths ("opang-$\Delta\phi$" gate). Finally, events of interest are identified by a gate on the reconstructed missing mass. (region A in fig. 6).

6.3 Beam- and Target Polarization, Luminosity

To deduce the spin correlation coefficients from the measured asymmetries (see sect. 7), the product P·Q of beam polarization P and target polarization Q has to be known. The analyzing power is measured as an asymmetry with either the target or the beam polarized. The product of the two asymmetries also depends on P·Q. Thus, P·Q is all one has to know about beam and target polarization. The product of beam and target polarization is determined, concurrently with the measurement of pion production, from spin correlation observables in pp elastic scattering near $90^\circ_{\mathrm{c.m.}}$.

Elastic scattering events are detected as coincidences between two opposite elements of scintillators S1−S4. Event reconstruction is based on the coordinates of both proton tracks in the first wire chamber (WC1). Since the angle between the two protons is known from kinematics, the polar angle of either prong is determined by the coordinates of the two tracks in just *one* plane (WC1). The event is recorded at the smaller of the two angles. Scattering angles in the range $37° \leq \theta_{\rm lab} \leq 42°$ are included.

For vertically polarized beam the measured, spin-dependent asymmetry is proportional to the (large) difference $A_\Delta \equiv A_{xx} - A_{yy}$ of two spin correlation parameters, (At 350 MeV e.g. $A_\Delta = -1.35$). For longitudinally polarized beam the measured, spin-dependent asymmetry is proportional to A_{zz} (at 350 MeV, $A_{zz} = 0.35$). The method of diagonal scaling [27] is used to analyze the data. This method minimizes systematic uncertainties due to spin-dependent differences in luminosity and due to variations in detector efficiency. The values used for the spin correlation parameters are based on the SM97 partial-wave analysis of the Virginia group [28]. The SM97 partial-wave analysis reproduces experimental values of the A_{ik} [13] within error (± 0.01), thus the absolute normalization of the data is linked to a measured calibration point [29].

The azimuthal angles φ of the two prongs, and thus the difference between them, $\Delta\varphi$, are also determined from the wire chamber information. The distribution of $\Delta\varphi$ consists of a large, narrow peak of coplanar pp events, superimposed on a broad distribution of non-coplanar background events. Events with $160° \leq \Delta\varphi \leq 200°$ were included in the data sample. The $\Delta\varphi$ distribution was used to determine the background underneath the peak at $\Delta\varphi$=180°. The broad distribution of background events was fitted to the left and to the right of the peak and the fraction underneath the peak was determined from the fit. For background events P·Q vanishes. The background was on the order of a few percent and resulted in an additive correction to the P·Q values of at most 0.02.

For an internal target in a stored beam it is difficult to measure separately the beam current and the target thickness with sufficient accuracy to derive a luminosity. Instead, the integrated luminosity is obtained from pp elastic scattering, observed concurrently with pion production. The differential cross section for pp scattering used is based on the SM97 partial-wave analysis of the Virginia group [28]. The numerical values have been obtained from the SAID interactive program [30]. The 45° detectors do not see the full length of the target (see fig. 3). To facilitate calculation of the solid angle the detector acceptance is restricted in software. Azimuthally, the acceptance is limited to a φ-range of $\pm 12°$. The vertex region was restricted to -2 cm $\leq z_0 \leq$ $+3$ cm, and the scattering angle is restricted to $40° \leq \theta_{\rm lab} \leq 42°$. The fraction of the target within the acceptance of the S-detectors is deduced from the vertex distribution z_0. The result of this analysis is a value for the integrated luminosity which is used only to verify that various mechanisms for the loss of events are understood and does not enter the extraction of polarization observables. Integrated luminosities in each of the individual spin states are also determined for diagnostic purposes.

7 Corrections

7.1 Detector Acceptance

In pion production near threshold, the nucleons are all within a forward cone that can be covered with a detector stack such as the one described here. However, there is still a dead zone due to the beam pipe hole in the center of the detectors.

To study the acceptance of the detector system for a given reaction at a given bombarding energy, a Monte Carlo program is used. It contains the detailed geometry of target and detectors, and includes the effects of multiple scattering, energy loss, the discrete positions obtained from the wire chambers, energy and time resolution of the scintillators, and the triangular target density distribution. Systematic effects, such as beam shifts, may be studied as well. The three-body final state is taken to be phase-space distributed with the option to include the final-state interaction between the two outgoing protons via an effective range expansion [31,32], and, for non-zero angular momentum in the final state, the expected dependence on the particle energies in the final state.

The Monte Carlo code generates simulated events in a format which is identical to that generated by the data acquisition system. These records are then processed with the same analysis software that is used for real data. This facilitates easy comparison of simulated and experimental data and also provides a convenient way to test the data acquisition software.

The Monte Carlo simulation was used to evaluate different mechanisms to lose events. For example, some events escape detection, because a valid trigger is not possible if the two protons fall into the same segment. The resulting inefficiency was on the order of a few percent. At 400 MeV, approximately 3% of $pp \to pp\pi^0$ events are not detected, because protons punch through both the E- and the K-detector and are thus vetoed by the V-detector. These inefficiencies are small and are usually unimportant in the determination of polarization observables. A more serious event loss is caused by the central hole that accommodates the circulating beam, causing a dead region around the beam axis of about 5° opening angle. For the $\mathrm{pp}\pi^0$ reaction this loss is sizeable because *both* protons must be outside the dead zone. Between 325 MeV and 400 MeV the fraction of lost, phase-space distributed events varies between 30% and 22%, respectively.

Since a polarization observable is a ratio of yields, an acceptance loss has an effect only if this observable for the lost events differs from that of the observed events. This is indeed the case for instance for the spin-dependent total cross section $\Delta\sigma_{\mathrm{T}}$. This observable reflects the mix of exit channels with different angular momentum (Ss, Ps, Pp). The probability of losing an event due to the hole also depends on the final state quantum numbers. Since these lost events can be calculated with the Monte Carlo code, a correction of $\Delta\sigma_{\mathrm{T}}$ due to the hole can be deduced.

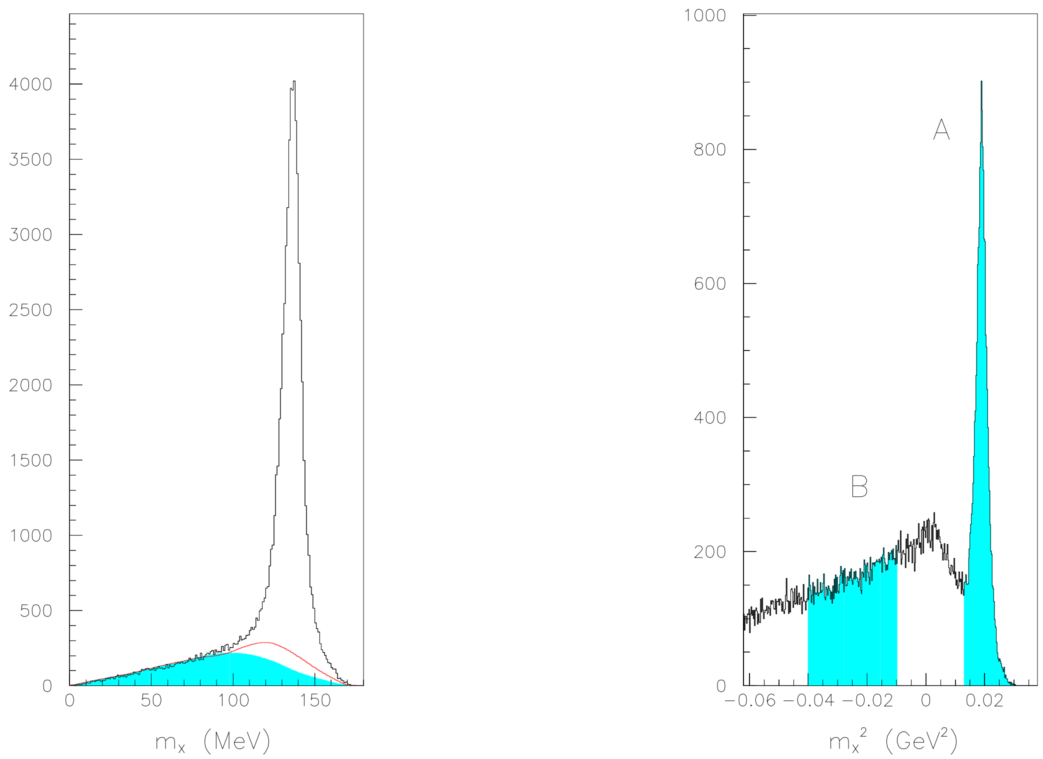

Fig. 6. Pion production events plus background at 375 MeV - distributions by missing mass m_x (left) and by m_x^2 (right). In the right spectrum, the “opang-$\Delta\phi$” gate (see condition 4 in sect. 6.2) has not been applied to admit a large fraction of background events. With the gate applied (left) the background events beneath the pion peak are seen to contribute a few percent to the peak area. The shaded area shows a spline fit to data taken with nitrogen gas in the cell, normalized to the left side of the event distribution. The smooth line is a similiar fit to a representative Monte Carlo background process simulation ($^{14}N + p \rightarrow^{12} B + 3p$).

7.2 Background

For the reaction $pp \to pp\pi^0$ two protons are required within the angular acceptance of the detector, and with an energy of less that 200 MeV (given the stopping power of the E and K detectors). In addition, a number of conditions are imposed (see sect. 6.2) and the calculated missing mass, m_x, is constrained to be near the mass of a pion (region A in the right panel of fig. 6). It turns out that there are many events with proton pairs within the accepted energy and angle range, that originate from reactions of protons on heavier nuclei, contained, for instance, in the walls of the target cell. The calculated m_x for these reactions can be seen as a broad distribution in figure 6. Since for such events the calculation of m_x is based on the incorrect assumption of a $p+p$ initial state, the result can even be imaginary ($m_x^2 < 0$). A small fraction of these events is clearly also present in the region of the pion mass peak, representing an unwanted contribution to the measured events of interest. The fraction of unwanted events is determined from the shape of the mass distribution of the background and its normalization, determined from the missing mass spectrum to the left of the peak.

The shape of the m_x distribution of the background events is well reproduced by a measurement in which the target gas was replaced by N_2 gas (shaded area in the left panel of fig. 6). It is also similiar to a Monte Carlo simulated response of our detector to reactions with a phase-space-distributed final state consisting of three or more protons and a nucleus with atomic number between 10 and 20 (smooth curve in the left panel of fig. 6). It is noteworthy that $(p, 2p)$ reactions do not significantly contribute because at least one of the two protons has an energy in excess of 200 MeV. The high-energy endpoint of the m_x distribution of background events increases with bombarding energy, increasing the background under the pion mass peak. On the other hand, the $pp \to pp\pi^0$ cross section grows more rapidly with energy, so that the fraction of background in the peak is largest at low bombarding energies.

From the direction of the two outgoing protons, the spatial distribution of the reaction vertices can be reconstructed. For events that originate in the target gas, the vertex distribution along the beam (z direction) is triangular, since the target gas enters the cell in the middle (at z=0) and the ends of the cell are exposed to pumping. This is illustrated in the upper-left panel of figure 7 which shows the vertex z-distribution for events in the mass peak (region A in right panel of fig. 6). The vertex distribution in the transverse plane for these events (lower-left part of fig. 7) shows a clean beam spot well inside the target cell (indicated by the circle). For background events (region B in right panel of fig. 6), the vertices are broadly distributed in the z direction (upper-right part of fig. 7). The transverse distribution in this case (lower-right part of fig. 7) shows spots on the cell wall, presumably from beam halo intercepting the cell

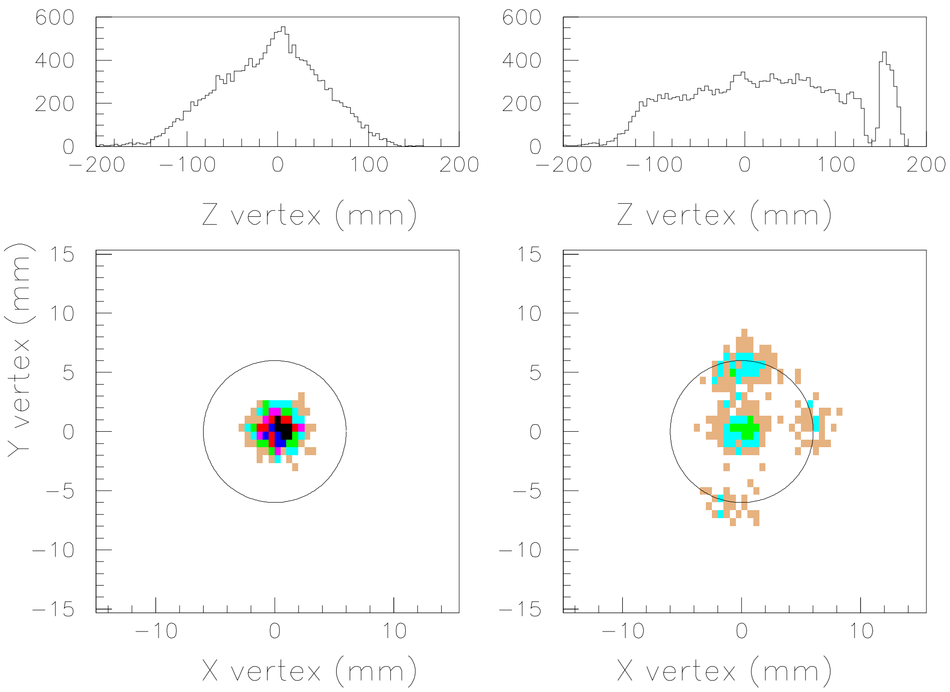

Fig. 7. (left) Distribution of reaction vertices for events of interest (region A in fig. 6). The upper panel shows the distribution along the beam. The fill tube is at z = 0, and the ends of the cell are at z = ±120 mm. The lower panel shows the distribution in a plane normal to the beam. The circle indicates the cell wall. For the transverse distribution a subset of the data from the downstream part of the cell is selected, because the position resolution is better closer to the detectors. (right) Same as left, but for the background events in region B in fig. 6

structure. In addition, there is also background originating from the position of the beam, suggesting impurities in the target gas. The z distribution of these events is found to have the shape of a parabola that reaches zero at the ends of the cell. From this fact, we conclude that the source for background which is localized at the beam is not an impurity in the atomic H beam but is rather due to out-gassing of the cell wall, and is thus distributed uniformly along the entire length of the cell. From the known out-gassing rate of Teflon we determine an impurity density of only about 1% of the density of the H target atoms. On the other hand, an estimate of the cross section for a reaction on a medium-weight nucleus which leads to two protons that fall into the pion mass region yields a value of the order of 1 mb, larger than the $pp \to pp\pi^0$ cross section by 1-2 orders of magnitude . These figures are consistent with the observed background from gas impurities.

The subtraction of unwanted events in the peak region is based on an assumption of the shape of the m_x distribution of the background. The shape given (see left panel of fig. 6) by measurements with N_2 target gas (shaded area) and Monte Carlo simulations (smooth curve). The difference between these two hypotheses suggests that multiple background processes may be present. In the analysis, the nitrogen curve is subtracted to obtain the pion yield, with the difference between the two background curves taken as a measure of the systematic error in the subtraction. The subtracted background is further constrained by the condition that spin correlation effects have to vanish for background reactions. The validity of the background subtraction method is tested by obtaining consistent results for the corrected observables when varying the limits of the pion peak region, and thus the background fraction.

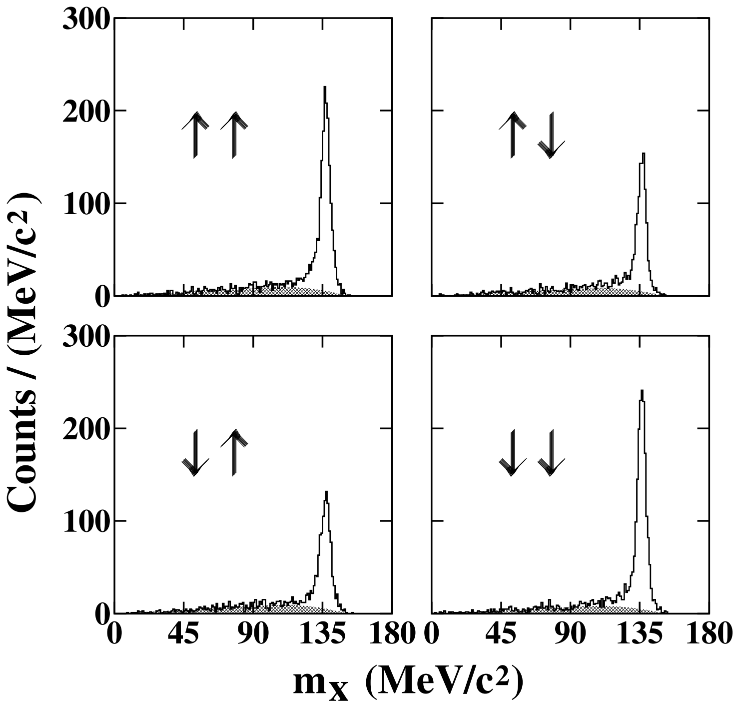

Fig. 8. Spin sorted missing mass spectra of the unobserved π^0 for transverse target and beam polarizations.

8 Summary

The PINTEX apparatus described in this paper has been constructed to measure, close to threshold, the dependence of the reactions $\vec{p}\vec{p} \to pp\pi^0$, $\vec{p}\vec{p} \to pn\pi^+$, and $\vec{p}\vec{p} \to d\pi^+$ on the spin of the colliding protons (see fig. 8, 9). The experimental setup has developed from the one used in the earlier total cross section measurement of $pp \to pp\pi^0$, and contains several of the original elements. The major new feature is the polarized target, and considerable effort has been invested during the past five years to learn about an internal polarized target in a storage ring, about its performance, about

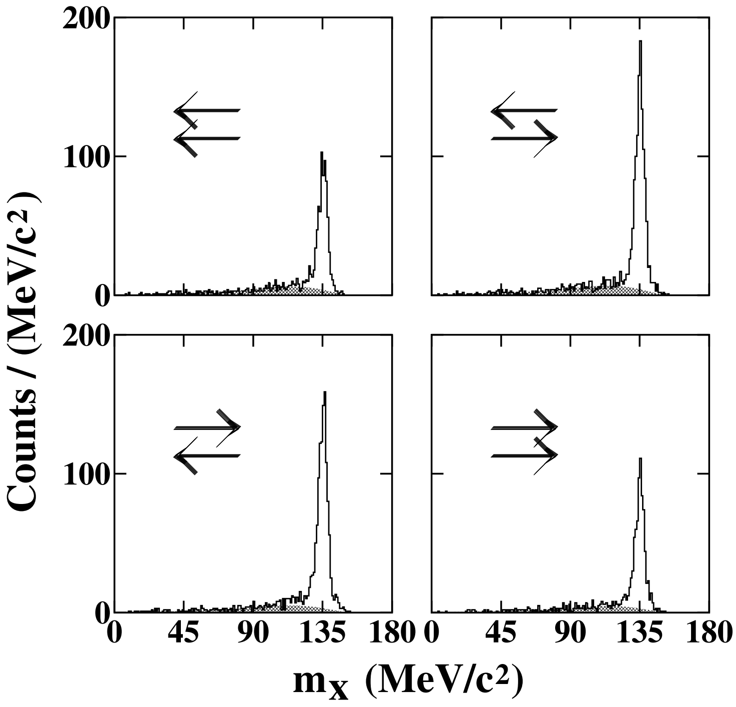

Fig. 9. Spin sorted missing mass spectra of the unobserved π^0 for longitudinal target and beam polarizations.

calibration procedures, and about the importance of a number of possible systematic effects and uncertainties. These studies were done in the context of a measurement of analyzing powers and spin correlation coefficients in pp elastic scattering (refs. [23], [24], [13]).

It is clear that polarization studies in pion production near threshold depend crucially on the advantages offered by internal target experiments. At this time this facility at IUCF is the unique place where such measurements can be carried out. The application of the apparatus to pion production, so far, consists of several runs of a total of about six weeks. Some early results for polarization observables in $pp \to pp\pi^0$ have been published (ref. [33]), but much more information will become available in the near future. In the future, this facility will be used to extend pion production studies to the three-nucleon system. Possible new detector developments include a small-angle detector which would improve the phase space coverage for $pd \to t\pi^+$.

Obviously, polarization is equally important in studies of near-threshold production of heavier mesons. This, however, is not within the reach of the IUCF Cooler. At COSY efforts to provide a polarized beam and a polarized target is underway [35]. Many of the lessons learned during pion production at IUCF will be helpful, but new problems will arise. One of these concerns the detection of more energetic ejectiles, since the use of stopping detectors becomes impractical for ejectile energies beyond 500 MeV.

Acknowledgements

We wish to thank IUCF accelerator operations group, in particular G. East and T. Sloan. This work was supported in part by the National Science Foundation and the United States Department of Energy.

References

[1] T. Ellison et al., IEEE Trans. Nucl. Sci. **NS-30**, 2636 (1983).

[2] H. Poth, Physics Reports, **196**, 135-297 (1990).

[3] R.E. Pollock, Annu. Rev. Nucl. Part. Sci. **41**, 357-88 (1991).

[4] H.O. Meyer, Annu. Rev. Nucl. Part. Sci. **47**, 235-71 (1997).

[5] H.O. Meyer et al., Nucl. Phys. **A539**, 633-61 (1992).

[6] A. Bondar et al., Phys. Lett. **B356**, 8-12 (1995).

[7] T. Sato et al., Phys. Rev. **C56**, 1246 (1997).

[8] C. Hanhart et al., Phys. Lett. B, in print, nucl-th/9808020.

[9] V. Derenchuk et al., American Inst. of Physics, AIP Conference Proceedings, 72-75 (1994).

[10] A. Pei, *Cooled RF Stacking Injection in the IUCF Cooler*, Ph.D. thesis, Indiana University (1991).

[11] H. O. Meyer et al., Phys. Rev. **E56**, 3578 (1997).

[12] R.E. Pollock, Phys. Rev. **E55**, 7606 (1997).

[13] B.v. Przewoski, Phys. Rev. **C58**, 1897 (1998).

[14] Hans Grote and F.Christoph, *The MAD Program (Methodical Accelerator Design)*, CERN/SL/90-13 (AP).

[15] B. Lorentz et al., Submitted to Phys. Rev. Lett.

[16] T. Wise, A.D. Roberts and W. Haeberli, Nucl. Instr. and Meth. **A336** 410(1993).

[17] A.D. Roberts, P.Elmer, T. Wise and W. Haeberli, Nucl. Instr. and Meth. **A322**, 6 (1992).

[18] S. S. Hanna, Proc. 4^{th} Int. Symp. on Polarization Phenomena in Nuclear Reactions, Basel, 1976.

[19] W. Haeberli, Proc. Workshop on Nuclear Phsics with Stored, Cooled Beams, AIP COnf. Proc. 128, 251 (1985).

[20] H.O. Meyer, *Polarized target and beam in a ring: Design constraints*, Workshop on Polarized Beams and Polarized Gas Targets, Cologne, Germany June 6-9 (1995), World Scientific, ISBN 981-02-2592-X.

[21] M.A. Ross et al., Nucl Instr. and Meth. **A326**, 424 (1993).

[22] J. S. Price and W. Haeberli, Nucl. Instr. and Meth. **A349**, 321 (1994).

[23] W. Haeberli et al., Phys. Rev. **C55**, 597 (1997).

[24] F. Rathmann et al., Phys. Rev. **C58**, 658 (1998).

[25] K. Solberg et al., Nucl. Instr. and Meth. **A281**, 283-90 (1989).

[26] W.W. Daehnick et al., Nucl. Instr. and Meth. **A320**, 2290 (1992).

[27] H.O. Meyer, Phys. Rev. **C56**, 2074 (1997).

[28] R.A. Arndt, C.H. Oh, I.I. Strakovsky, R.L. Workmann, F. Dohrmann, Phys. Rev. **C56**, 3005 (1997).

[29] B.v. Przewoski et al., Phys. Rev. **C44**, 44 (1991).

[30] The SAID dial-in: available via TELNET to clsaid.phys.vt.edu, with userid:said (no password required).

[31] K.M. Watson , Phys. Rev. **88**, 1163 (1952).

[32] A.B. Migdal , Sov. Phys. JETP **1**, 2 (1955).

[33] H.O. Meyer, Phys. Rev. Lett **81**, 3096 (1998).

[34] H.O. Meyer, Proc. 8th Int. Conf. on the Structure of the Baryons, Bonn, 22-26 Sep (1998).

[35] Institut für Kernphysik and COSY, Annual Report 1997, report no. 3505, Forschungstentrum Jülich, 1998.